Inspiral-Merger-Ringdown Waveforms for Black-Hole Binaries with Nonprecessing Spins

P. Ajith, M. Hannam, S. Husa, Y. Chen, B. Brügmann, N. Dorband, D. Müller, F. Ohme, D. Pollney, C. Reisswig, L. Santamaría, and J. Seiler

Phys. Rev. Lett. **106**, 241101 — Published 15 June 2011

DOI: 10.1103/PhysRevLett.106.241101

Inspiral-merger-ringdown waveforms for black-hole binaries with non-precessing spins

P. Ajith,[1,2] M. Hannam,[3,4] S. Husa,[5] Y. Chen,[2] B. Brügmann,[6] N. Dorband,[7]
D. Müller,[6] F. Ohme,[7] D. Pollney,[7,5] C. Reisswig,[7,2] L. Santamaría,[7,1] and J. Seiler[7]

[1]*LIGO Laboratory, California Institute of Technology, Pasadena, CA 91125, USA*
[2]*Theoretical Astrophysics, California Institute of Technology, Pasadena, CA 91125, USA*
[3]*Gravitational Physics, Faculty of Physics, University of Vienna, Boltzmanngasse 5, A-1090 Vienna, Austria*
[4]*School of Physics and Astronomy, Cardiff University, Queens Building, CF24 3AA, Cardiff, United Kingdom*
[5]*Departament de Física, Universitat de les Illes Balears, Crta. Valldemossa km 7.5, E-07122 Palma, Spain*
[6]*Theoretisch-Physikalisches Institut, Friedrich Schiller Universität Jena, Max-Wien-Platz 1, 07743 Jena, Germany*
[7]*Max-Planck-Institut für Gravitationsphysik (Albert-Einstein-Institut), Am Mühlenberg 1, 14476 Golm, Germany*

We present the first analytical inspiral-merger-ringdown gravitational waveforms from binary black holes (BBHs) with non-precessing spins, that is based on a description of the late-inspiral, merger and ringdown in full general relativity. By matching a post-Newtonian description of the inspiral to a set of numerical-relativity simulations, we obtain a waveform family with a conveniently small number of physical parameters. The physical content of these waveforms include the "orbital hang-up" effect, and "spin flips". These waveforms will allow us to detect a larger parameter space of BBH coalescence, including a considerable fraction of precessing binaries in the comparable-mass regime, thus significantly improving the expected detection rates.

Coalescing black-hole (BH) binaries are among the most promising candidate sources for the first detection of gravitational waves (GWs). Such observations will lead to precision tests of general relativity as well as provide a wealth of information relevant to fundamental physics, astrophysics, and cosmology. Computation of the expected waveforms from these sources is a key goal in current research in gravitation.

While the *inspiral* and *ring-down* stages of the BH coalescence are well-modeled by perturbative techniques, an accurate description of the *merger* requires numerical solutions of Einstein's equations. Although performing numerical simulations densely sampling the entire parameter space of BH coalescence is computationally prohibitive, waveform templates modeling all the three stages can now be constructed by combining analytical- and numerical- relativity results, dramatically improving the sensitivity of searches for GWs from BH binaries, and the accuracy of estimating the source parameters [1–4]. To date, inspiral-merger-ringdown (IMR) templates have been computed only for nonspinning BH binaries [1, 3–6]. However, most BHs in nature are expected to be spinning [7], which necessitates the inclusion of spinning-binary waveforms in GW searches. But, spin adds six parameters (three components for each BH), and each additional parameter in a search template bank leads to a higher signal-to-noise-ratio (SNR) threshold for a confident detection [8]. Also, this requires accurate numerical simulations across this large parameter space, which are not yet available. Moreover, implementing a search covering the full spin parameter space has proven to be difficult.

In this letter, we present an IMR waveform family modeling the dominant harmonic of binaries with non-precessing spins, i.e., spins (anti-)aligned with the orbital angular momentum. Aligned-spin binaries are an astrophysically interesting population as such systems are expected from isolated binary evolution and in gas-rich galactic mergers [9, 10]. Non-precessing binaries also exhibit interesting strong-gravity effects like the "orbital hang-up" [11] and "spin flips" [12]. We make use of the degeneracies in the physical parameters to parametrize our waveform family by only the total mass $M \equiv m_1+m_2$ of the binary, the symmetric mass ratio $\eta \equiv m_1 m_2/M^2$, and a *single* spin parameter $\chi \equiv (1+\delta)\chi_1/2 + (1-\delta)\chi_2/2$, where $\delta \equiv (m_1-m_2)/M$ and $\chi_i \equiv S_i/m_i^2$, S_i being the spin angular momentum of the ith BH. The last feature is motivated by the observation (see e.g., [13]) that the leading spin-orbit-coupling term in post-Newtonian (PN) waveforms is dominated by this parameter. We also show that this waveform family is able to capture a significant fraction of precessing binaries in the comparable-mass regime, providing an efficient and feasible way of searching for these systems [35].

Numerical simulations.— Binary BH (BBH) waveforms covering at least eight wave cycles before merger were produced by solving Einstein equations numerically, as written in the "moving-puncture" 3+1 formulation [14, 15]. The numerical solutions were calculated with the `BAM` [16, 17], `CCATIE` [18] and `LLAMA` [19] codes. Initial momenta were chosen to give low-eccentricity inspiral, using either an extension of the method described in [20], or the quasicircular formula used in [21]. GWs were extracted at $R_{ex} = 90M$ with `BAM`, $R_{ex} = 160M$ with `CCATIE` and at future null infinity with `LLAMA`, using procedures discussed in [16, 18, 22]. In all simulations the GW amplitude is accurate to *at least* 10% and the phase to *at least* 1 radian over the duration of the simulation. Most of the waveforms employed in the construction of the analytical templates are significantly longer (12–22 cycles) and more accurate [23].

We used seven sets of simulations: (1) Equal-mass binaries with equal, non-precessing spins $\chi_i = \pm\{0.25, 0.5, 0.75, 0.85\}$, described in [23, 24]. (2) Non-precessing, equal-spin binaries with $q \equiv m_1/m_2 = \{2, 2.5, 3\}$ and $\chi_i = \{\pm 0.5, 0.75\}$. (3) Nonspinning binaries with $q = \{1, 1.5, 2, 2.5, 3, 3.5, 4\}$. (4) Unequal-spin binaries with $q = \{2, 3\}$ and $(\chi_1, \chi_2) = (-0.75, 0.75)$. (5) Equal-mass, unequal-spin binaries with $\chi_i = \pm\{0.2, 0.3, 0.4, 0.6\}$. (6) Equal-mass, precessing binaries with spin vectors $(0.42, 0, 0.42), (0, 0, 0)$ and

$(0.15,0,0),(0,0,0)$. (7) Precessing $q=3$ binary with spins $(0.75,0,0),(0,0,0)$. Simulation sets (1)–(4) and (7) were performed with `BAM`, set (5) with `CCATIE`, and set (6) with `LLAMA`. The analytical waveform family is constructed employing *only* the equal-spin simulation sets (1)–(3); sets (4)–(7) were used to test the efficacy of our model against more general spin/mass configurations. Two additional waveforms were used in these tests: the Caltech-Cornell equal-mass, non-spinning simulation [25], and the RIT $q=1.25$ precessing binary simulation with $|\chi_1|=0.6, |\chi_2|=0.4$ [26].

Constructing hybrid waveforms.— We produce a set of "hybrid waveforms" [5] by matching PN and numerical-relativity (NR) waveforms in an overlapping time interval $[t_1,t_2]$. These hybrids are assumed to be the target signals that we want to detect. For the PN inspiral waveforms we choose the "TaylorT1" waveforms at 3.5PN [27] phase accuracy, considering spin terms up to 2.5PN [13, 28]. This is motivated by PN-NR comparisons of equal-mass spinning binaries, in which the accuracy of the TaylorT1 approximant was found to be the most robust [23, 24]. We include the 3PN amplitude corrections to the dominant quadrupole mode [29] and the 2PN spin-dependent corrections [13], which greatly improved the agreement between PN and NR waveforms. For precessing waveforms, spin and angular momenta are evolved according to [28, 30].

We match the PN and NR waveforms by doing a least-square fit over time- and phase shifts between the waveforms, and a scale factor a that reduces the PN-NR amplitude difference [5]. The NR waveforms are combined with the "best-matched" PN waveforms in the following way: $\mathrm{h}^{\rm hyb}(t) \equiv a\tau(t)\,\mathrm{h}^{\rm NR}(t) + (1-\tau(t))\,\mathrm{h}^{\rm PN}(t)$, where $\mathrm{h}(t) = h_+(t) - i h_\times(t)$ and τ ranges linearly from zero to one for $t\in[t_1,t_2]$.

Waveform templates for non-precessing binaries.— The analytical waveforms that we construct are written in the Fourier domain as $h(f)\equiv A(f)\,e^{-i\Psi(f)}$, where

$$A(f) \equiv C f_1^{-7/6} \begin{cases} f'^{-7/6}\,(1+\sum_{i=2}^{3}\alpha_i\,v^i) & \text{if } f<f_1 \\ w_m\,f'^{-2/3}\,(1+\sum_{i=1}^{2}\epsilon_i\,v^i) & \text{if } f_1\le f<f_2 \\ w_r\,\mathcal{L}(f,f_2,\sigma) & \text{if } f_2\le f<f_3, \end{cases}$$

$$\Psi(f) \equiv 2\pi f t_0 + \varphi_0 + \frac{3}{128\,\eta\,v^5}(1+\sum_{k=2}^{7} v^k\,\psi_k). \qquad (1)$$

Above, $f'\equiv f/f_1$, $v\equiv(\pi M f)^{1/3}$, $\epsilon_1 = 1.4547\,\chi - 1.8897$, $\epsilon_2 = -1.8153\,\chi + 1.6557$ (estimated from hybrid waveforms), C is a numerical constant whose value depends on the sky-location, orientation and the masses, $\alpha_2 = -323/224 + 451\,\eta/168$ and $\alpha_3 = (27/8 - 11\,\eta/6)\chi$ are the PN corrections to the Fourier domain amplitude of the ($\ell=2, m=\pm2$ mode) PN waveform [13], t_0 is the time of arrival of the signal at the detector and φ_0 the corresponding phase, $\mathcal{L}(f,f_2,\sigma)$ a Lorentzian function with width σ centered around the frequency f_2, w_m and w_r are normalization constants chosen so as to make $A(f)$ continuous across the "transition" frequencies f_2 and f_1, and f_3 is a convenient cutoff frequency such that the signal power above f_3 is negligible. The phenomenological parameters ψ_k and $\mu_k \equiv \{f_1, f_2, \sigma, f_3\}$ are written in terms of the physical parameters of the binary as:

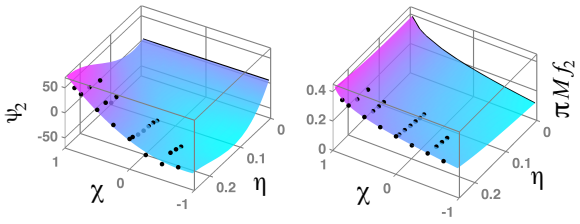

FIG. 1: Phenomenological parameters ψ_2 and f_2 computed from *equal-spin* hybrid waveforms (dots), fits given by Eq. (2) (surfaces), and the test-mass limit (black traces). Total mass, symmetric mass ratio and spin parameter are denoted by M,η and χ.

$$\psi_k = \sum_{i=1}^{3}\sum_{j=0}^{N} x_k^{(ij)}\,\eta^i\chi^j + \psi_k^0\,, \quad \pi M\mu_k = \sum_{i=1}^{3}\sum_{j=0}^{N} y_k^{(ij)}\,\eta^i\chi^j + \mu_k^0\,, \qquad (2)$$

where $N\equiv\min(3-i,2)$ while $x_k^{(ij)}$ and $y_k^{(ij)}$ are tabulated in Table I. Figure 1 plots an example of this map from the phenomenological- to physical- parameter space.

We match these waveforms to 2PN accurate adiabatic inspiral waveforms in the test-mass ($\eta\to0$) limit, where the phenomenological parameters reduce to:

$$f_1\to f^0_{\rm LSO},\;\; f_2\to f^0_{\rm QNM},\;\; \sigma\to f^0_{\rm QNM}/Q^0,\;\; \psi_k\to\psi_k^0. \qquad (3)$$

Above, $f^0_{\rm LSO}$ and $f^0_{\rm QNM}$ are the frequencies of the last stable orbit [31] and the dominant quasi-normal mode, and Q^0 is the ring-down quality factor [32] of a Kerr BH with mass M and spin χ, while ψ_k^0 are the (2PN) Fourier domain phasing coefficients of a test-particle inspiralling into the Kerr BH, computed using the stationary-phase approximation [13].

The test-mass-limit waveforms suffer from two limitations: 1) we assume that the evolution of the GW phase at the merger and ringdown stages is a continuation of the adiabatic inspiral phase, and 2) in the absence of a reliable plunge model, we approximate the amplitude of the plunge with $f'^{-2/3}\,(1+\sum_{i=1}^{2}\epsilon_i\,v^i)$. Nevertheless, in the test-mass limit, it is expected that the signal will be dominated by the long inspiral stage, and the inspiral is guaranteed to be well-modelled by our waveforms. More importantly, the imposition of the appropriate test-mass limit in our fitting procedure ensures that the waveforms are well behaved even outside the parameter range where current NR data are available. Because of this, and the inclusion of the PN amplitude corrections, these waveforms are expected to be closer to the actual signals than the templates proposed in [1, 6] in the non-spinning limit. However, since the parameter space covered by the NR simulations is limited, we recommend that these waveforms be used only in the regime $q\lesssim10$ and $-0.85\lesssim\chi\lesssim0.85$. Also, these are meant to model only the late-inspiral, merger and ring down ($M f_{\rm GW} > 10^{-3}$), i.e., signals from binaries in the mass-range where merger-ringdown also contribute to the SNR, apart from inspiral.

	Test-mass limit (ψ_k^0)	$x^{(10)}$	$x^{(11)}$	$x^{(12)}$	$x^{(20)}$	$x^{(21)}$	$x^{(30)}$
ψ_2	3715/756	-920.9	492.1	135	6742	-1053	-1.34×10^4
ψ_3	$-16\pi + 113\chi/3$	1.702×10^4	-9566	-2182	-1.214×10^5	2.075×10^4	2.386×10^5
ψ_4	$15293365/508032 - 405\chi^2/8$	-1.254×10^5	7.507×10^4	1.338×10^4	8.735×10^5	-1.657×10^5	-1.694×10^6
ψ_6	0	-8.898×10^5	6.31×10^5	5.068×10^4	5.981×10^6	-1.415×10^6	-1.128×10^7
ψ_7	0	8.696×10^5	-6.71×10^5	-3.008×10^4	-5.838×10^6	1.514×10^6	1.089×10^7
	Test-mass limit (μ_k^0)	$y^{(10)}$	$y^{(11)}$	$y^{(12)}$	$y^{(20)}$	$y^{(21)}$	$y^{(30)}$
f_1	$1 - 4.455(1-\chi)^{0.217} + 3.521(1-\chi)^{0.26}$	0.6437	0.827	-0.2706	-0.05822	-3.935	-7.092
f_2	$[1 - 0.63(1-\chi)^{0.3}]/2$	0.1469	-0.1228	-0.02609	-0.0249	0.1701	2.325
σ	$[1 - 0.63(1-\chi)^{0.3}](1-\chi)^{0.45}/4$	-0.4098	-0.03523	0.1008	1.829	-0.02017	-2.87
f_3	$0.3236 + 0.04894\chi + 0.01346\chi^2$	-0.1331	-0.08172	0.1451	-0.2714	0.1279	4.922

TABLE I: Phenomenological parameters describing the analytical waveforms. In test-mass limit, they reduce to the appropriate quantities given by perturbative calculations [13, 31, 32]. The test-mass limit of f_1 is a fit to the frequency of the last stable orbit given in [31].

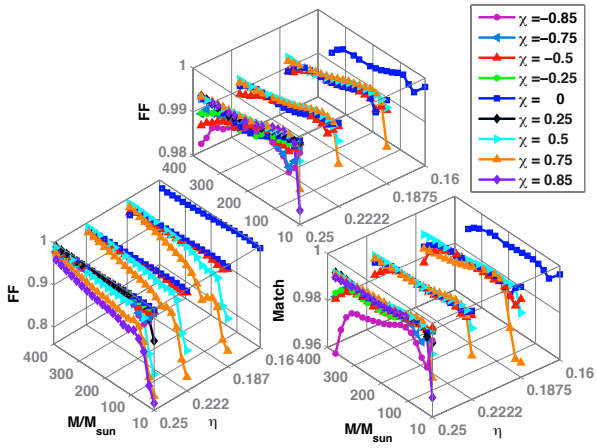

FIG. 2: *Top and right plots*: Match and FF of our analytical IMR templates with equal-spin hybrid waveforms constructed from simulation sets (1)–(3). *Bottom left*: FF of *non-spinning* IMR templates proposed in [1, 6] with the same hybrids. A comparison with the other plots demonstrates the effect of neglecting spins.

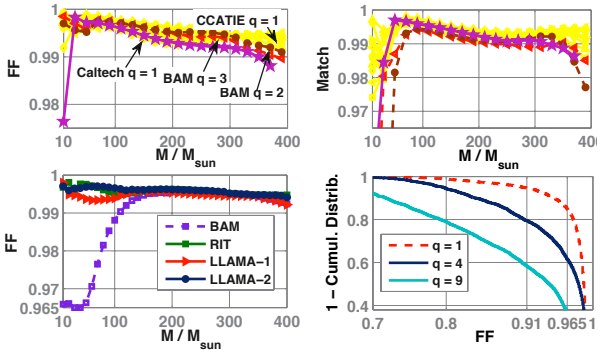

FIG. 3: *Top panel:* Match and FF of the our templates with *unequal-spin* hybrid waveforms constructed from simulation sets (4) and (5), and the Caltech-Cornell non-spinning simulation. *Bottom left:* FF with *precessing* hybrids constructed from sets (6) and (7), and the RIT simulation. *Bottom right:* Fraction of generic precessing PN waveforms ($M = 10M_\odot$) producing fitting factor FF with the templates proposed in this paper — 85% (62%) 37% of the binaries with $q = 1$ (4) 9 produce FF > 0.965.

We have examined the "faithfulness" [33] of the new templates in reproducing the hybrid waveforms by computing the *match* (noise-weighted inner product) with the hybrids. Loss of the SNR due to the "mismatch" between the template and the true signal is determined by the match maximized over the whole template bank – called *fitting factor* (FF). The standard criteria for templates used in searches is that FF > 0.965, which corresponds to a loss of no more than 10% of signals.

Match and FF of the analytical waveforms with the equal-(unequal-) spin hybrid waveforms are plotted in Fig. 2 (Fig. 3), using the Initial LIGO design noise spectrum [34]. Note that the analytical waveform family is constructed employing *only* the equal-spin hybrid waveforms (Fig. 2). The PN–NR matching region used to construct the unequal-spin hybrids (Fig. 3) are also different from that used for equal-spin hybrids. These figures demonstrate the efficacy of the analytical templates in reproducing the target waveforms – templates are "faithful" (match > 0.965) *either* when the masses *or* the spins are equal, while they are *always* "effectual" [33] in detection (FF > 0.965). In contrast, the bottom left plot of Fig. 2 shows the FF of the non-spinning IMR template family proposed in [1, 6] with the equal-spin hybrid waveforms. FFs as low as 0.8 suggest that up to 50% binaries may go undetected if nonspinning IMR templates are employed to search for binaries with high (aligned) spins.

The bottom left plot of Fig. 3 shows the FF and match of the template family with four *precessing* hybrid waveforms. The high FFs are indicative of the effectualness of the templates in detecting precessing binaries. Since presently not enough NR simulations are available to make a quantitative statement, and since we expect the effect of precession will be predominant in the case of lower mass binaries (when large number of cycles are present in the detector band), we might be able to acquire some useful indication by studying precessing PN waveforms. We performed a Monte-Carlo sim-

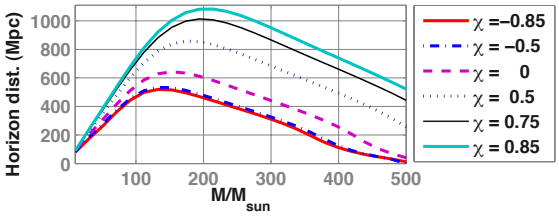

FIG. 4: Distance to optimally-located and oriented- equal-mass binaries with (equal) spin χ producing optimal SNR 8 in Initial LIGO.

ulation where we generate precessing "restricted" PN waveforms with $M = 10M_{\odot}$, $q = \{1, 4, 9\}$, uniformly distributed spin magnitudes in the interval $[0, 0.98]$ and isotropically distributed spin angles, and compute the FF with the templates proposed in this paper. The inclination of the binary's total angular momentum with the line of sight from the observer is also randomly chosen from $[0, \pi]$. The bottom right plot of Fig. 3 shows the cumulative distribution of the FF, strongly indicating the effectualness of the templates in detecting precessing binaries in the comparable-mass regime. These results indicate that a search employing non-precessing templates described by a single spin parameter might be an attractive and feasible way of searching for generic spinning binaries [36].

Distance to optimally oriented BBHs producing optimal SNR of 8 in Initial LIGO is shown in Fig. 4, which demonstrates the dramatic effect of spin for detection of high-mass binaries; if most BBHs are highly spinning, then LIGO will be able to detect BH coalescences up to 1Gpc, thus increasing the event rates as much as five times compared to predictions based on models of nonspinning binaries. For Advanced LIGO, the distance reach is as high as 20 Gpc.

Conclusions.— We combine state-of-the-art results from analytical- and numerical relativity to construct for the first time a family of analytical IMR waveforms for BBHs with non-precessing spins. These waveforms are also able to detect a significant fraction of the precessing binaries in the comparable-mass regime, with spins represented by a *single* parameter. This will considerably simplify the use of our waveforms in GW searches in the near future, and will accelerate the incorporation of NR results into the current effort for the first detection of GWs. There are many other immediate applications of our waveforms: injections into detector data will help to put more realistic upper limits on the rate of BBH coalescences, and to compare the different algorithms employed in the search for BBHs, while employing these in population-synthesis studies will provide more accurate coalescence rates observable by the current and future detectors. Our method can readily be generalized to incorporate non-quadrupole harmonics, larger portions of the BBH parameter space and further information from analytical approximation methods or numerical simulations.

SH was supported by VESF and EGO, DAAD grant D/07/13385 and Spanish Ministry of Science grant FPA-2007-60220. MH was supported by FWF grant M1178-N16 and STFC grant ST/H008438/1. PA and YC were supported by NSF grants PHY-0653653, PHY-0601459, PHY-0956189 and David and Barbara Groce Fund. BB is supported by DFG grant SFB/Transregio 7 "GW Astronomy", BB and DM by DLR, and LS by DAAD grant A/06/12630. We thank AEI, FSU Jena, LRZ, ICHEC, VSC, CESGA and BSC-CNS for computational resources, and K. G. Arun, B. Sathyaprakash, G. Faye and R. O'Shaughnessy for discussions.

[1] P. Ajith et al., Phys. Rev. D **77**, 104017 (2008).
[2] P. Ajith and S. Bose, Phys. Rev. D **79**, 084032 (2009).
[3] A. Buonanno et al., Phys. Rev. D **76**, 104049 (2007).
[4] T. Damour and A. Nagar, Phys. Rev. D **79**, 081503 (2009).
[5] P. Ajith et al., Class. Quant. Grav. **24**, S689 (2007).
[6] P. Ajith, Class. Quant. Grav. **25**, 114033 (2008).
[7] M. Volonteri et al., Astrophys. J. **620**, 69 (2005).
[8] C. Van Den Broeck et al., Phys. Rev. D **80**, 024009 (2009).
[9] V. Kalogera, Pramana **63**, 673 (2004).
[10] T. Bogdanović, C. S. Reynolds, and M. C. Miller, Astrophys. J. **661**, L147 (2007).
[11] M. Campanelli et al., Phys. Rev. D **74**, 041501(R) (2006).
[12] A. Buonanno et al., Phys. Rev. D **77**, 026004 (2008).
[13] K. G. Arun et al., Phys. Rev. D **79**, 104023 (2009).
[14] M. Campanelli et al., Phys. Rev. Lett. **96**, 111101 (2006).
[15] J. G. Baker et al., Phys. Rev. Lett. **96**, 111102 (2006).
[16] B. Brügmann et al., Phys. Rev. D **77**, 024027 (2008).
[17] S. Husa et al., Class. Quant. Grav. **25**, 105006 (2008).
[18] D. Pollney et al., Phys. Rev. D **76**, 124002 (2007).
[19] D. Pollney et al., Phys. Rev. D **83**, 044045 (2011).
[20] S. Husa et al., Phys. Rev. D **77**, 044037 (2008).
[21] B. Brügmann et al., Phys. Rev. D **77**, 124047 (2008).
[22] C. Reisswig et al., Phys. Rev. Lett. **103**, 221101 (2009).
[23] M. Hannam et al., Phys. Rev. D **82**, 124008 (2010).
[24] M. Hannam et al., Phys. Rev. D **78**, 104007 (2008).
[25] M. A. Scheel et al., Phys. Rev. D **79**, 024003 (2009).
[26] M. Campanelli et al., Phys. Rev. D **79**, 084010 (2009).
[27] L. Blanchet et al., Phys. Rev. Lett. **93**, 091101 (2004).
[28] L. Blanchet, A. Buonanno, and G. Faye, Phys. Rev. D **74**, 104034 (2006), gr-qc/0605140v4.
[29] L. Blanchet et al., Class. Quant. Grav. **25**, 165003 (2008).
[30] A. Buonanno et al., Phys. Rev. D **67**, 104025 (2003).
[31] J. M. Bardeen et al., Astrophys. J. **178**, 347 (1972).
[32] F. Echeverria, Phys. Rev. D **40**, 3194 (1989).
[33] T. Damour et al., Phys. Rev. D **57**, 885 (1998).
[34] http://www.ligo.caltech.edu/~jzweizig/distribution/LSC_Data.
[35] The reason is that the (spin-dependent) phase evolution is primarily governed by the spin-orbit coupling, determined by the spin components along the angular momentum.
[36] These results hold for Enhanced LIGO also.